

20030108157

This Document  
Reproduced From  
Best Available Copy

①

PHYSICAL MODELING TECHNIQUES FOR MISSILE  
AND OTHER  
PROTECTIVE STRUCTURES

ADA130328

Papers Submitted for Presentation During the  
American Society of Civil Engineers  
National Spring Convention  
Las Vegas, April 1982

Sponsored By the ASCE Engineering Mechanics Division  
Committee on Experimental Analysis and Instrumentation

Edited By: T. Krauthammer and C. D. Sutton

DTIC  
JUL 14 1983  
A

This document has been approved  
for public release and sale; its  
distribution is unlimited.

DTIC FILE COPY

83 02 028 008



DEPARTMENT OF THE AIR FORCE  
HEADQUARTERS BALLISTIC MISSILE OFFICE (AFSC)  
NORTON AIR FORCE BASE CALIFORNIA 92409

PA

29 Jun 83

Review of Material for Public Release

Mr. James Shafer  
Defense Technical Information Center  
DDAC  
Cameron Station  
Alexandria, VA 22314

The following technical papers have been reviewed by our office and are approved for public release. This headquarters has no objection to their public release and authorizes publication.

1. (BMO 81-296) "Protective Vertical Shelters" by Ian Narain, A.M. ASCE, Jerry Stepheno, A.M. ASCE, and Gary Landon, A.M. ASCE.
2. (BMO 82-020) "Dynamic Cylinder Test Program" by Jerry Stephens, A.M. ASCE.
3. (AFCMD/82-018) "Blast and Shock Field Test Management" by Michael Noble.
4. (AFCMD/82-014) "A Comparison of Nuclear Simulation Techniques on Generic MX Structures" by John Betz.
5. (AFCMD/82-013) "Finite Element Dynamic Analysis of the DCT-2 Models" by Barry Bingham.
6. (AFCMD/82-017) "MX Basing Development Derived From H. E. Testing" by Donald Cole.
7. (BMO 82-017) "Testing of Reduced-Scale Concrete MX-Shelters-Experimental Program" by J. I. Daniel and D. M. Schultz.
8. (BMO 82-017) "Testing of Reduced-Scale Concrete MX-Shelters-Specimen Construction" by A. T. Ciolko.
9. (BMO 82-017) "Testing of Reduced-Scale Concrete MX-Shelters-Instrumentation and Load Control" by N. W. Hanson and J. T. Julien.
10. (BMO 82-003) "Laboratory Investigation of Expansion, Venting, and Shock Attenuation in the MX Trench" by J. K. Gran, J. R. Bruce, and J. D. Colton.

11. (BMO 82-003) "Small-Scale Tests of MX Vertical Shelter Structures" by J. K. Gran, J. R. Bruce, and J. D. Colton.

12. (BMO 82-001) "Determination of Soil Properties Through Ground Motion Analysis" by John Frye and Norman Lipner.

13. (BMO 82-062) "Instrumentation for Protective Structures Testing" by Joe Quintana.

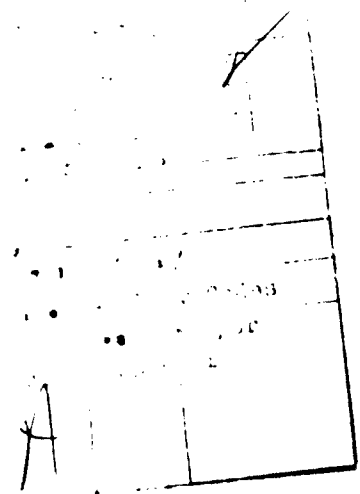
14. (BMO 82-105) "1/5 Size VHS Series Blast and Shock Simulations" by Michael Noble.

15. (BMO 82-126) "The Use of Physical Models in Development of the MX Protective Shelter" by Eugene Sevin.

\*16. REJECTED: (BMO 82-029) "Survey of Experimental Work on the Dynamic Behavior of Concrete Structures in the USSR" by Leonid Millstein and Gajanan Sabnis.

  
CAROL A. SCHALKHAM, LTC, USAF  
Public Affairs Officer

Cy To: Dr. T. Krauthammer  
Associate Professor  
Department of Civil and  
Mineral Engineering  
University of Minnesota



FINITE ELEMENT DYNAMIC ANALYSIS  
OF DCT-2 MODEL E

by

B. L. Bingham, 1st Lt, USAF  
DTC Project Officer  
Air Force Weapons Laboratory  
Structural Dynamics Section

ABSTRACT

This report discusses quasi three-dimensional finite element dynamic analysis performed for a buried reinforced concrete cylindrical shell explosive test conducted by AFWL at Kirtland AFB, NM. The test (conducted on 27 Feb 81) included two horizontal ICBM shelter models with rectangular roof cut-outs, inner steel liners, longitudinal interior rails, and two different thickness to inner radius ratios (0.18 and 0.28). Both models were subjected to a combined axial and transverse simulated nuclear environment. The finite element analysis examines the axial response to include the initial compressive wave, structure-media interaction loads, longitudinal vertical bending, axial strains and motion, and effects of certain structural details such as rectangular roof cutouts and varying thickness to internal radius ratio. The reinforced concrete material model is piecewise linear, perfectly plastic with smeared steel.

Key Words: Dynamic Structural Response, Horizontal Buried Cylinders, Finite Element Analysis, Axial Response, Longitudinal Bending, Structural Modeling.

C

# FINITE ELEMENT DYNAMIC ANALYSIS OF DCT-2 MODEL E

by Barry L. Bingham<sup>1</sup>

## INTRODUCTION

### Background

Shallow buried, scaled horizontal cylindrical shelters for Inter-Continental Ballistic Missiles (ICBMs) were subjected to a simulated nuclear airblast environment. This test, the second Dynamic Cylinder Test (DCT-2) subjected these generic horizontal shelter models to a combined axial and transverse airblast environment. This shelter concept consists of a closure/headworks region which opens into a roadway and is directly subjected to airblast loading. The rest of the cylinder is covered by soil berm. The closure/headworks region is elevated above the front roadway such that the soil directly underneath the shelter is loaded. Each of the models in DCT-2 contained two rectangular roof cut-outs (called Strategic Arms Limitation Talks, SALT, ports). These ports are designed for removal for missile verification. The models also have inner steel liners, longitudinal support beams near the springline to support a missile mass simulator, and two different thickness to inner radius ratios ( $T/IR = 0.18$  and  $0.28$ ). Posttest data analysis of DCT-2 concluded that a low frequency longitudinal vertical bending moment dominated structural response with moment concentration occurring at the first SALT port.

### Analysis Objectives

The objective of the SAMSON (Ref. 1) two dimensional (quasi three-dimensional) finite element dynamic analysis of a 1/4.22 scale generic horizontal shelter is to examine and define axial response in a combined axial and transverse loading environment. Specific items of interest in axial response include the initial longitudinal compressive wave down the length of the model, the reflected relief wave off the backwall, axial strains and motion, structure-media interaction (SMI) loads,

---

<sup>1</sup>Structural Dynamics Research Engineer, 1st Lt, USAF, at the Air Force Weapons Laboratory, Civil Engineer Research Division, Structural Response Section, Kirtland AFB, New Mexico.

longitudinal vertical bending, and effects of certain structural details such as SALT ports.

#### Scope

A SAMSON two dimensional (2-D) finite element computer code calculation was performed to simulate the response of DCT-2 structure E (T/IR = 0.18). The 2-D model was subjected to axial and transverse waveforms determined to be best fits to DCT-2 environmental data. This model is very simple to use and inexpensive to run, while being extensive and reliable in information gained. It is capable of simulating longitudinal structural motion, longitudinal structural strains, longitudinal near field soil motion, SMI shear stresses, SMI normal stresses, vertical soil motion and stresses, and structural ovaling. Each of the structural parameters vary from crown to invert. This report mainly focuses on comparison of the calculation results to test data. An AFWL technical report yet to be published (under the same name as this report) discusses theoretical development of this modeling procedure in greater detail.

### DESCRIPTION OF ANALYTICAL MODELING PROCEDURES

#### Finite Element Grid

The basic model configuration in the DCT-2 testbed is shown in Figure 1. The entire two dimensional SAMSON finite element grid (Figure 2) is a representation of the elevation view shown in Figure 1. The finite element grid can be separated into two main element groups; (1) the structural elements and (2) the soil elements.

There are 95 bilinear displacement quadrilateral structural elements and 120 structural nodes (Figure 2). The largest element dimension is 0.758 meter (29.8 in) and the smallest is 0.246 meter (9.7 in). A single element represents each of the two SALT port lids located at third points down the length of the structure. The SALT port joint gaps are represented by the element material properties. The tube section of the structure is represented by five layers of plane stress elements (Figure 3).

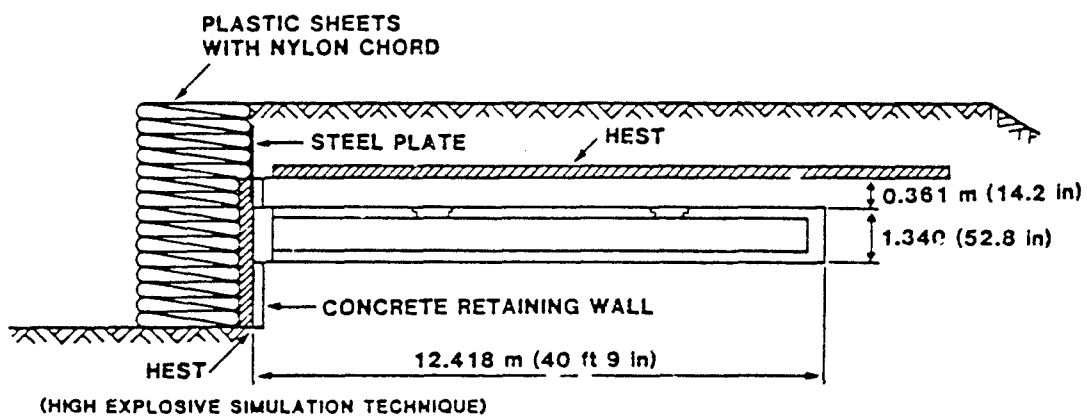


Figure 1. DCT-2 elevation view.

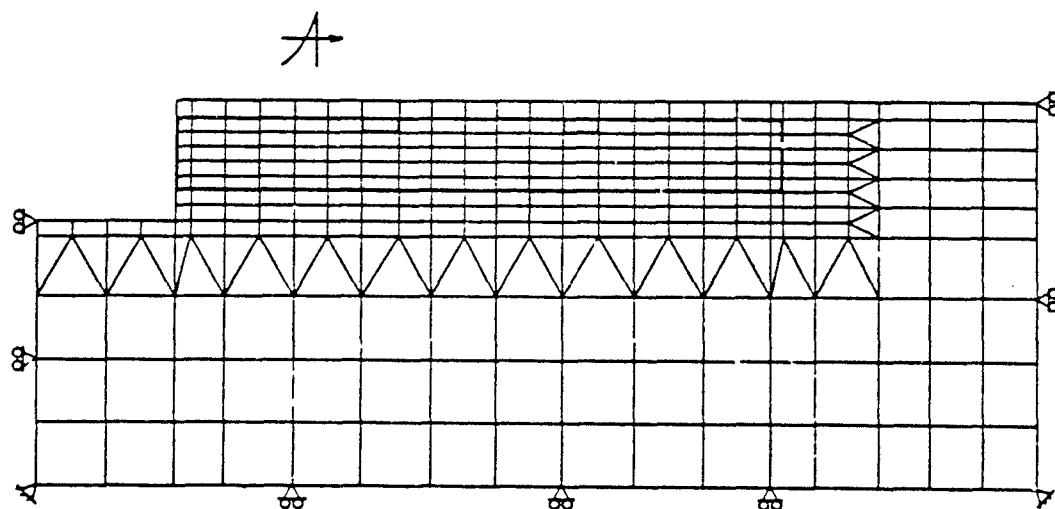


Figure 2. DCT-2 grid.

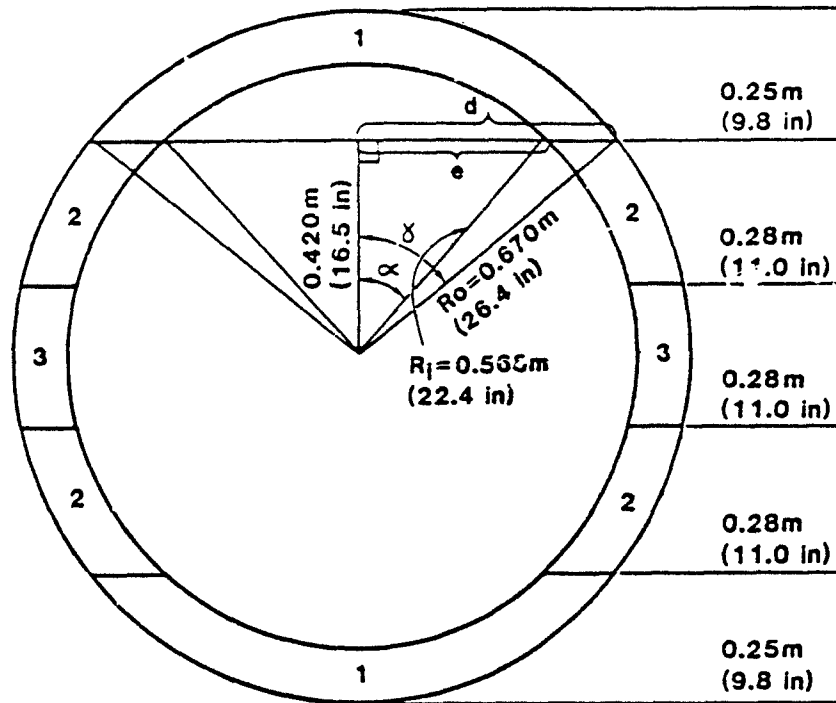


Figure 3. SAMSON 1 grid break-up DCT-2 Model E.

The structure sits in a soil island grid (Figure 2) which is simply supported along the bottom and outermost sides. There are 311 bilinear displacement quadrilateral soil elements and 320 soil nodes (Figure 2). The grid is 20.4 meters (66 ft 11.2 in) wide and 7.3 meters (23 ft 11.4 in) high. The largest element dimension is 1.394 meters (54.9 in) and the smallest is 0.246 meter (9.7 in). The soil elements make up a continuous grid with the structural elements overlaying soil elements. This type of grid allows for full development of ground shock from air-blast loading, while load is also being applied to the structure. There are seven sliding/separating boundaries (SSB) between the soil and structure elements. One SSB defines the interface at the backwall. The remaining six SSB's are all horizontal with respect to the grid in Figure 2 and extend down the entire length of the structure. The top and bottom SSB's are at the crown and invert, respectively, with the other four SSB's corresponding to the structural layers in between. The three SSB's above the structure springline are such that downward moving soil cannot pass through any of the SSB's, but the soil is free to move

upward. The three SSB's below the structure springline are such that downward motion of the structure is restricted by the soil. The elements on either side of the SSB can slide relative to each other, separate, and impact after separation. The SSB's transmit normal and shear forces at the nodes across the interface.

### Structural Modeling

The structure consists of five layers of tube elements, two SALT port elements, five loader lid elements, and five backwall elements. All of the structural elements are anisotropic with different material models in the horizontal (X) and vertical (Z) directions. The horizontal or longitudinal material model for the tube elements is shown in Figure 4. The axial reinforced concrete (R/C) behavior is represented by an elastic-plastic material model. The SALT port joint gap is represented by a 1.0 mm shift in the stress-strain curve and a zero tensile cutoff (Figure 5).

The vertical elastic modulus for the structure tube elements has to be modified to allow for ovaling of the cylinder. The equation for the vertical ovaling modulus,  $E_v$ , is derived in an Air Force Weapons Laboratory (AFWL) technical report yet to be published (under the same name as this report) from concepts presented in Timoshenko's "Theory of Plates and Shells" (Ref. 2, pp 5 and 502).

$$E_v = \frac{L}{A} \frac{EI}{0.149 a^3 (1-\nu^2)} \quad (1)$$

where

- L = Total depth of the structure elements (1.340 meters)
- A = Weighted average (with respect to the element vertical depths) of the element vertical areas for a 1.0 meters long section ( $0.295 \text{ m}^2$ )
- E = Young's Modulus for concrete ( $3.45 \times 10^4 \text{ MPa}$ )
- I = Area moment of inertia of a cracked wall cross section 1.0 meters long ( $2.66 \times 10^{-5} \text{ m}^4$ )
- a = Average cylinder radius (0.619 meter)

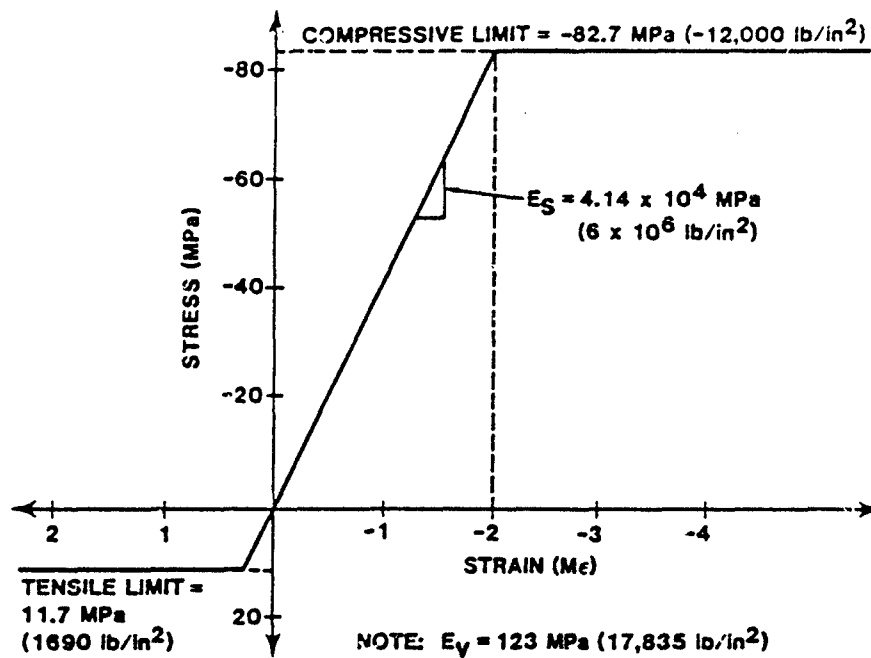


Figure 4. DCT-2 R/C material model.

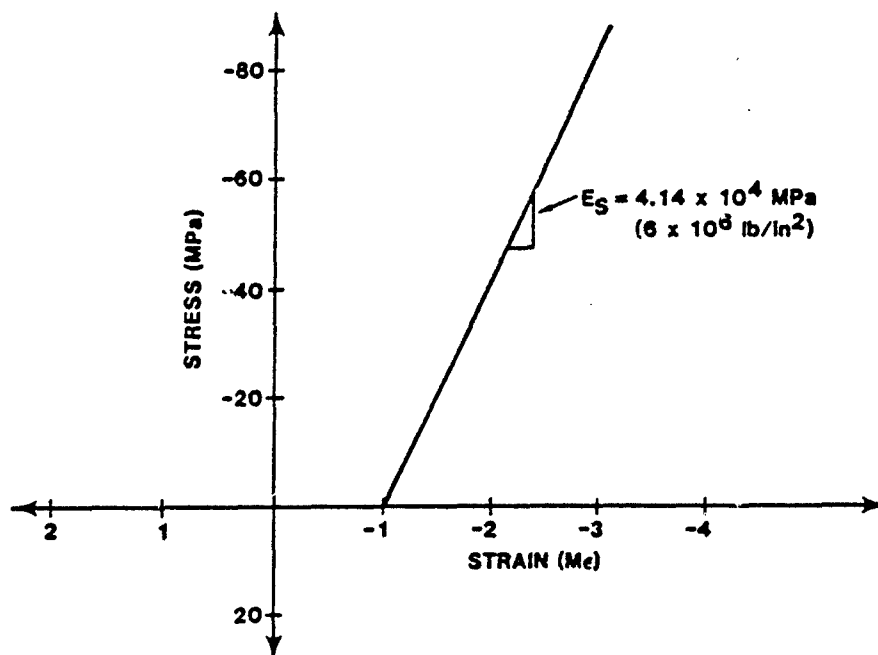


Figure 5. DCT-2 SALT port lid material model.

$\nu$  = Poisson's ratio for concrete (0.2)

$E_v$  = Ovaling modulus (123.0 MPa)

This vertical ovaling modulus resulted in the relative displacement between the crown and invert nodes (at mid structure) shown in Figure 6. The peak relative displacement is 26.5 mm (1.04 in) which is characteristic of DCT-2 test data.

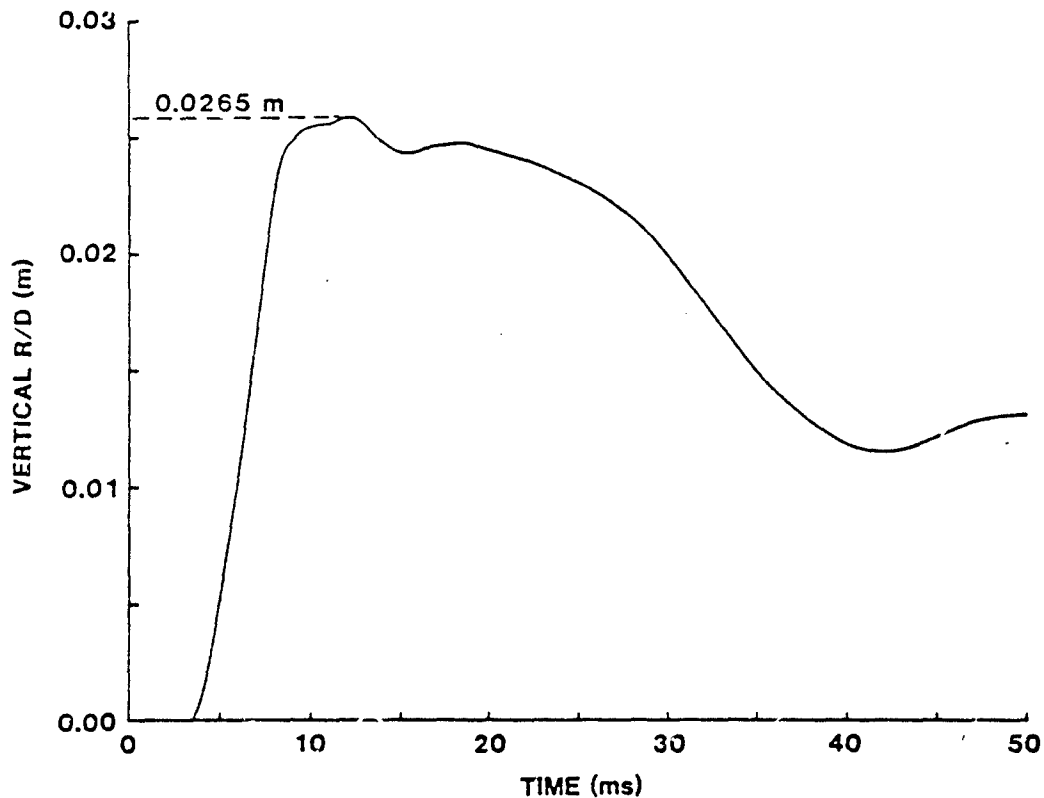


Figure 6. Relative displacement between crown and invert nodes at mid-structure.

#### Airblast Representation

Figure 7 shows the assessed axial and transverse loading environments for DCT-2. The pressure waveforms were input into SAMSON as pressure-time pairs (also shown in Figure 7). The transverse pressure waveform traveled over the top of the finite element grid (Figure 2) from left to right with a velocity of 2936 m/s (9630 ft/s). The axial pressure waveform was applied to the full layer of soil elements and the

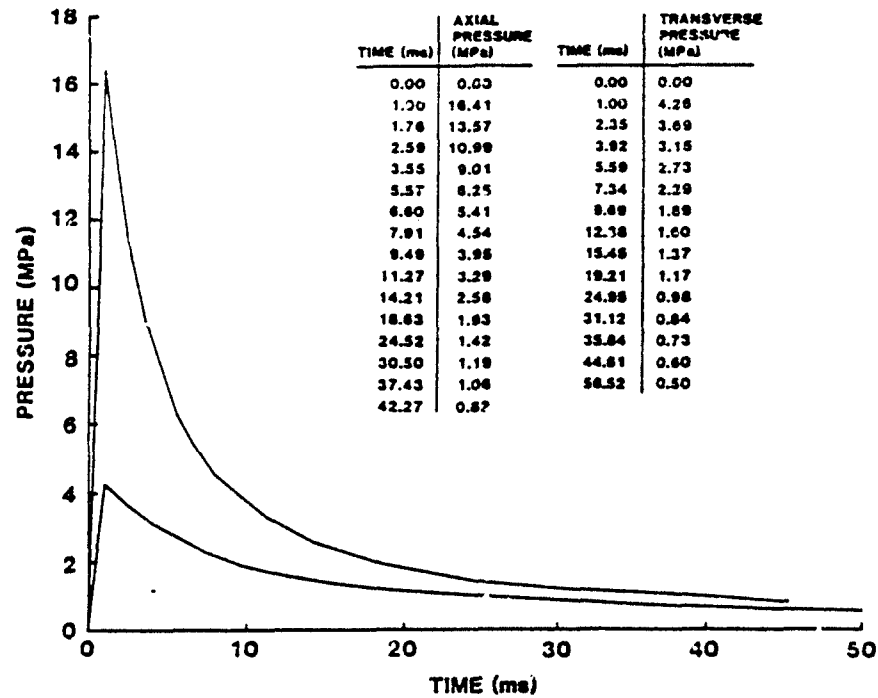


Figure 7. DCT-2 axial and transverse loading environments.

overlayed structural elements. The axial pressure waveform traveled over the front face of the soil and structure elements from top to bottom with a velocity of 6400 m/s (21000 ft/s).

#### COMPARISON OF ANALYSIS TO TEST DATA

##### Structure Response

DCT-2 test data relevant to the SAMSON calculation is in two categories; (1) longitudinal motion and (2) longitudinal strains.

##### Longitudinal Motion.

Longitudinal motion data from DCT-2 model E is rather limited. Gage placement only measured longitudinal motion in the structure at the springline and at seven locations along the length,  $x = 2.108$  meters, 4.159 meters, 6.209 meters, 7.799 meters, 8.259 meters, 9.284 meters, and 12.172 meters. Figure 8 compares the nearest SAMSON calculation plot (solid lines) to each of the measured data plots (dash dot lines).

In general the comparison is excellent. The first peak is matched very well in timing and magnitude. Between  $X = 2.109$  meters (6.9 ft) and  $X = 7.799$  meters (25.6 ft) (Figure 8 (a) - (d)) SAMSON tends to overestimate the magnitude of the second peak. There are three main possibilities for this discrepancy; (1) the calculation did not allow enough SMI shear damping, or (2) the structural damping coefficient (0.04) was too low, or (3) the gage measurements are in error after early time response (after 6.0 ms). As of this writing the above possibilities have not been thoroughly investigated. At  $X = 8.259$  meters (27.1 ft) and beyond (Figure 8 (e) - (g)) the second peak is matched very well in timing and magnitude.

#### Longitudinal Strains.

Figure 9 shows plots of DCT-2 E axial strains at seven locations along the length of the structure;  $X = 2.109$  meters, 3.699 meters, 4.159 meters, 5.184 meters, 6.209 meters, 8.259 meters, and 10.309 meters, respectively. Figure 10 shows the corresponding SAMSON strains. Comparing Figures 9 and 10 reveal many similarities. At approximately  $X = 2.1$  meters (Figure 9 (a) and 10 (a)) the axial strain at the crown has an initial peak strain followed by a larger second peak strain at 6.0 ms. This second peak strain is most likely due to initiation of vertical bending. The invert strain in Figure 9 (a) seems to be contrary to indicated response with the measurement showing compression rather than tension after 10.0 ms. At approximately  $X = 3.5$  meters (Figure 9 (b) and 10 (b)) and  $X = 4.1$  meters (Figure 9 (c) and 10 (c)) notice that the SAMSON calculation overestimates the initial peak strain at the crown. Therefore, the assumption of 1.0 me for the SALT port joint gap is most likely too low. In general after 5.0 ms in both the DCT-2 E and SAMSON data the highest compressive strains occur at the crown and the highest tensile strains occur at the invert. Other than this general view, timing coordination between the two sets of data is difficult. At approximately 5.0 meters on back timing of the peak bending moment seems to be in fair agreement between the two sets of data. Again, the invert measurement in Figure 9 (d) seems to be contrary to indicated response after 10.0 ms. The best agreement occurs at  $X = 6.209$  meters (Figure 9 (e) and 10 (e)) for timing and impulse of the initial peak compressive

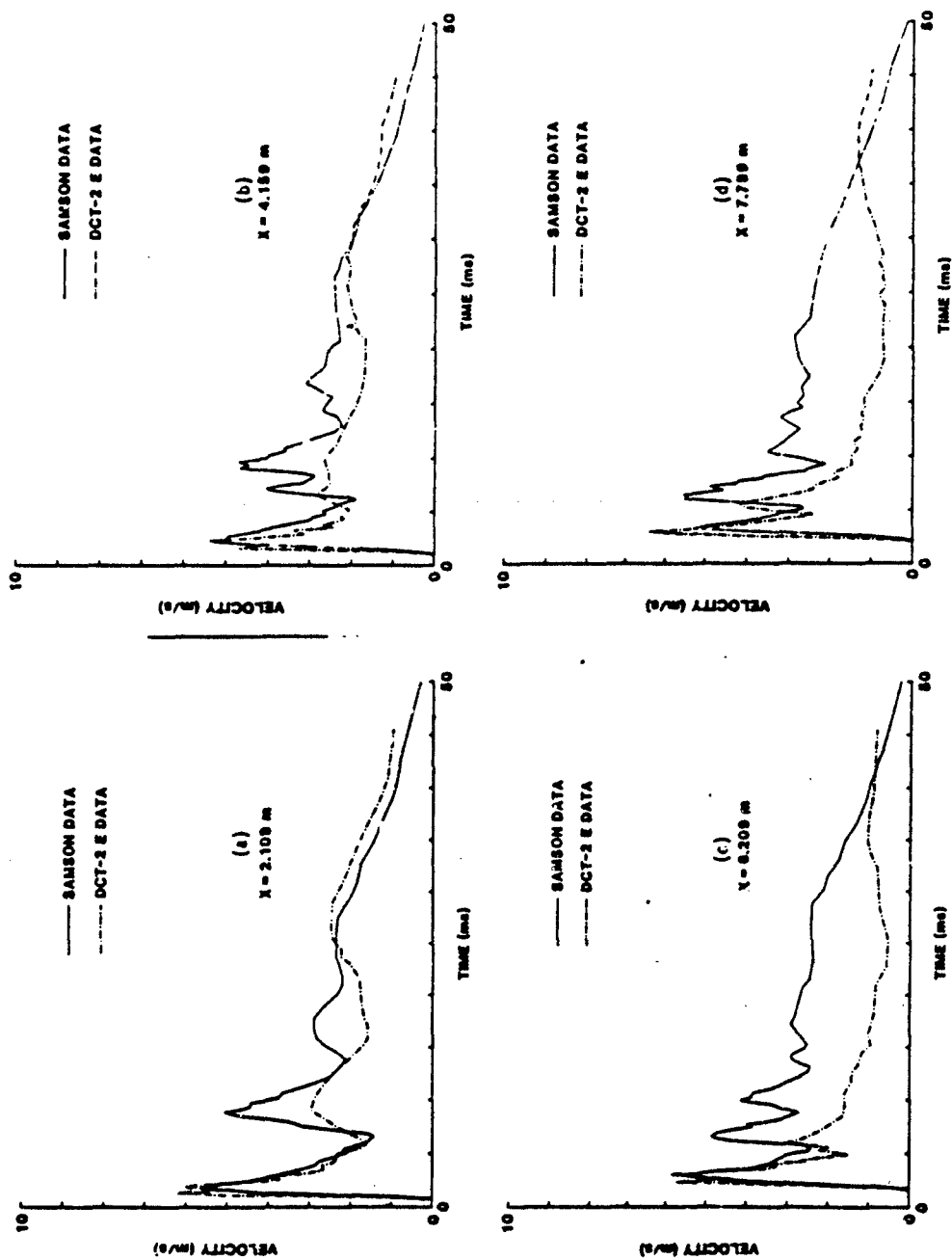


Figure 8. Comparison of longitudinal motion.

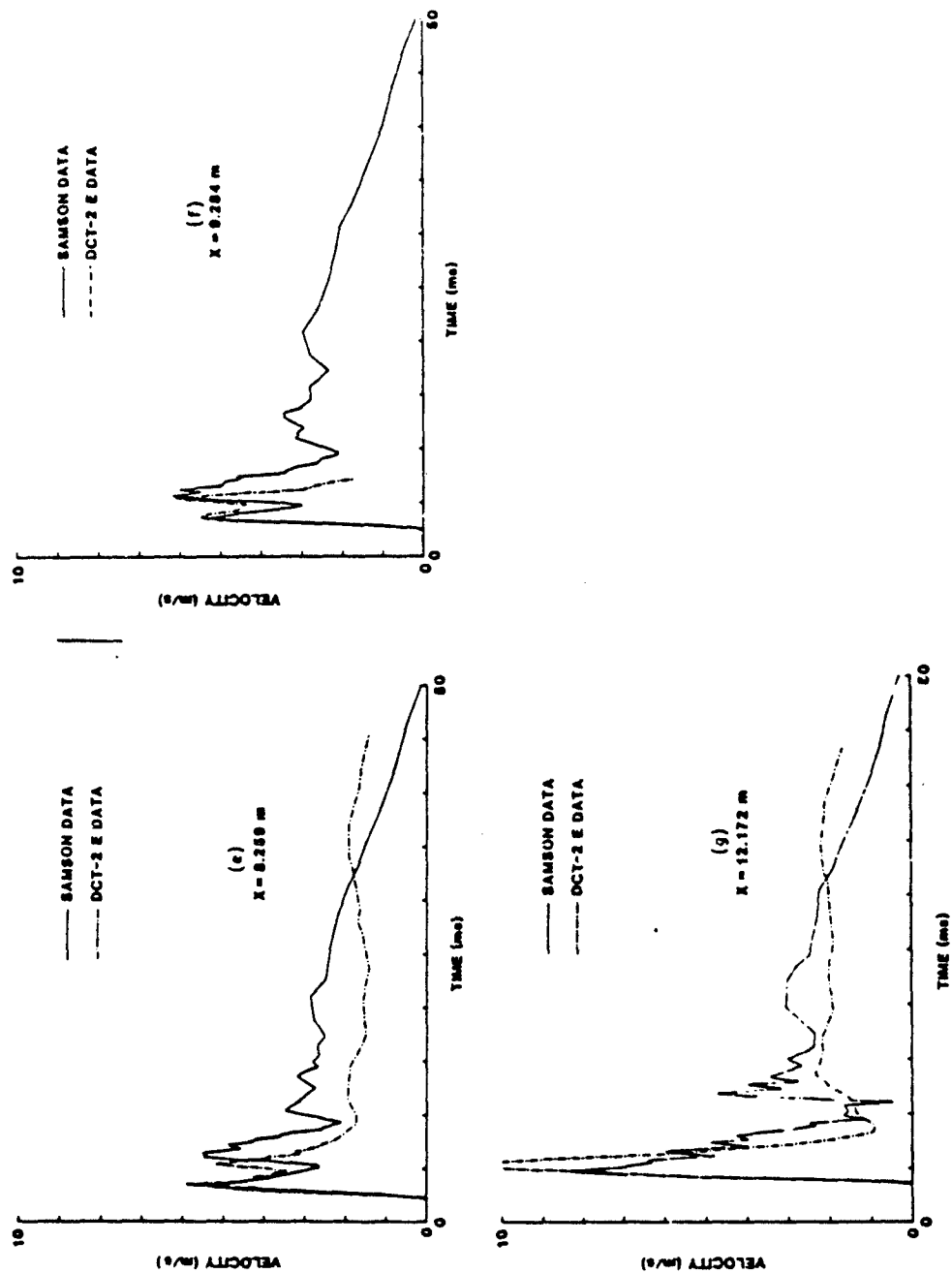


Figure 8. Comparison of longitudinal motion (continued).

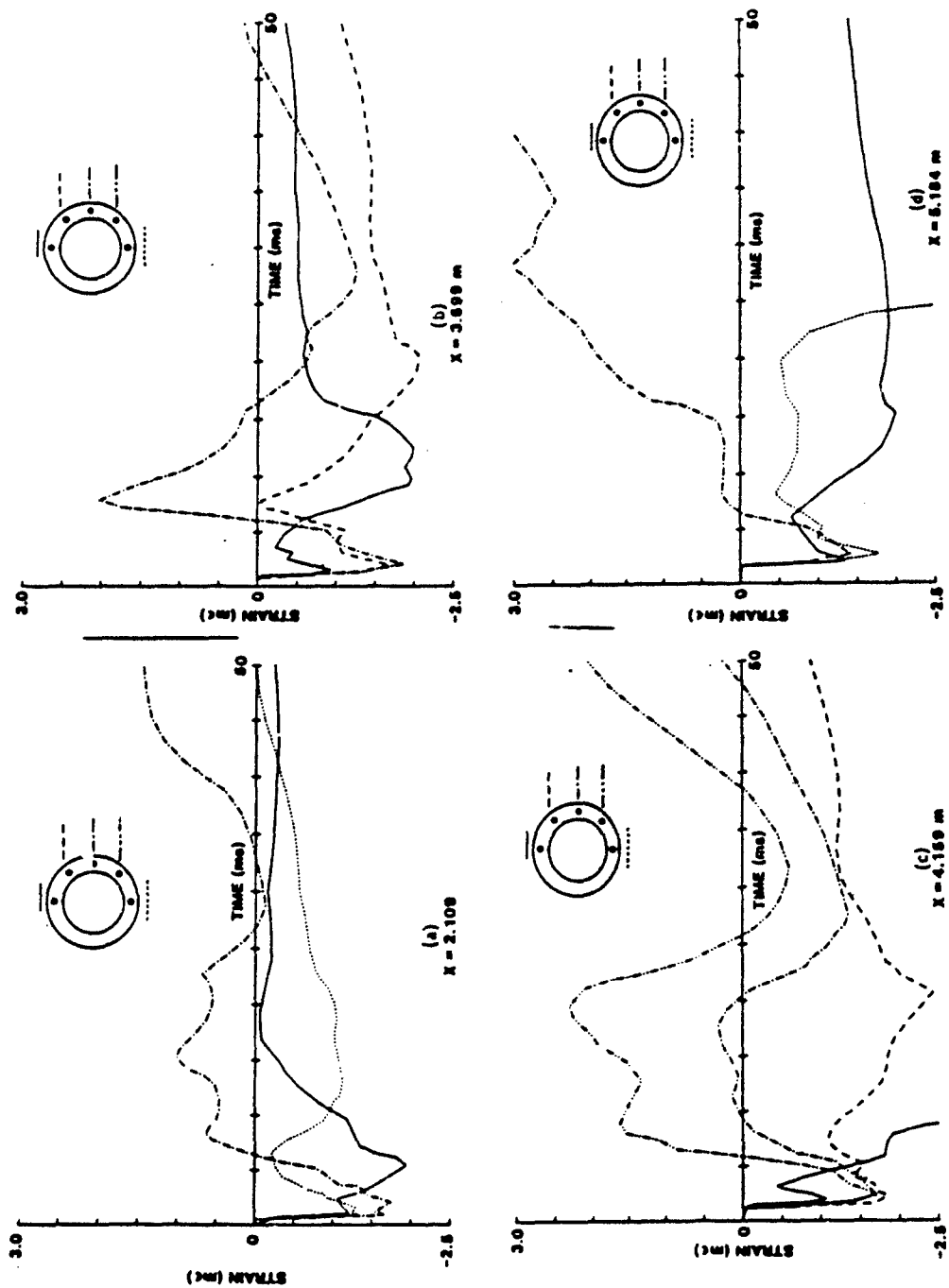


Figure 9. DCT-2 E axial strains.

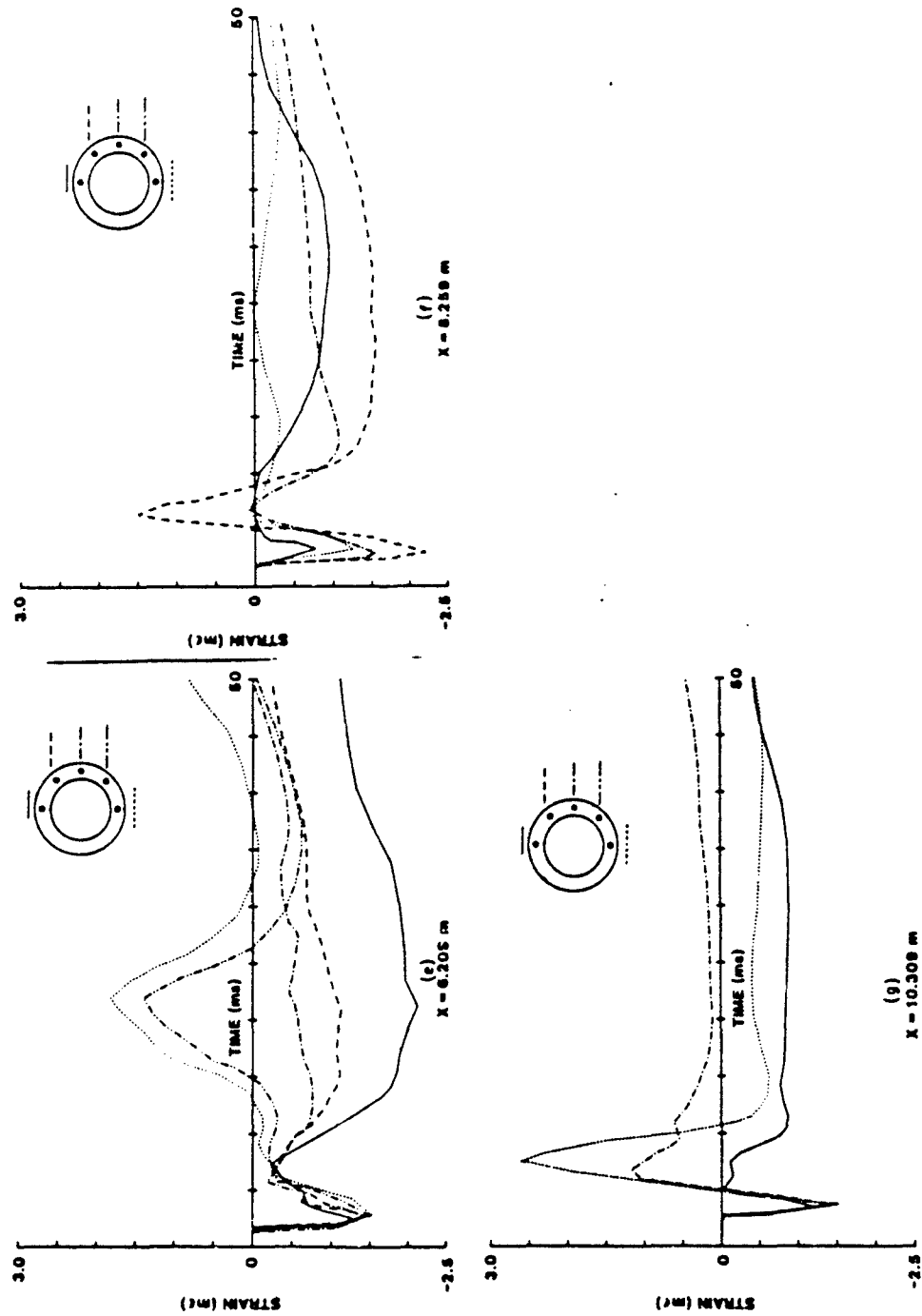


Figure 9. DCT-2 E axial strains (continued).

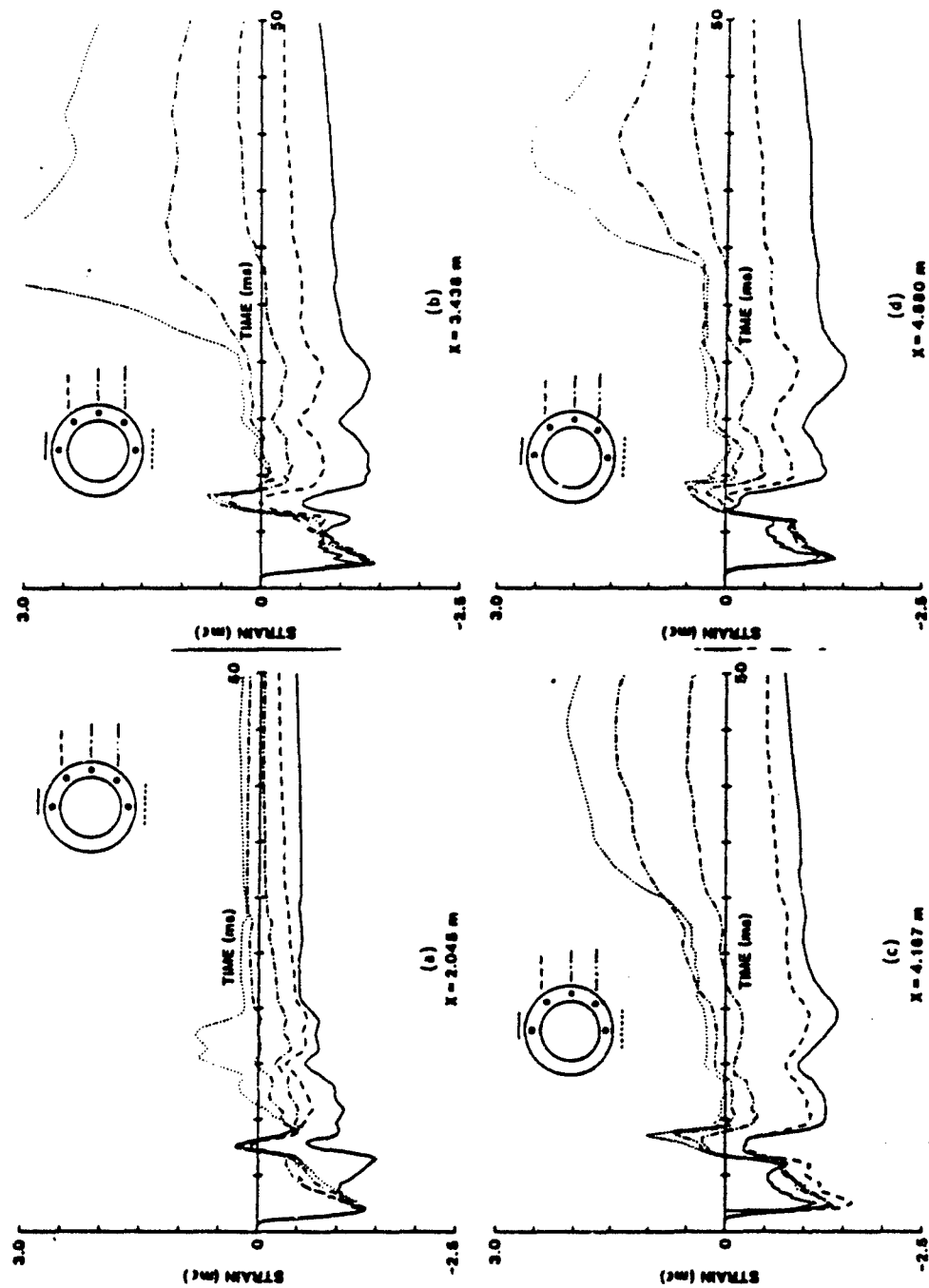


Figure 10. SAMSON structural axial strains.

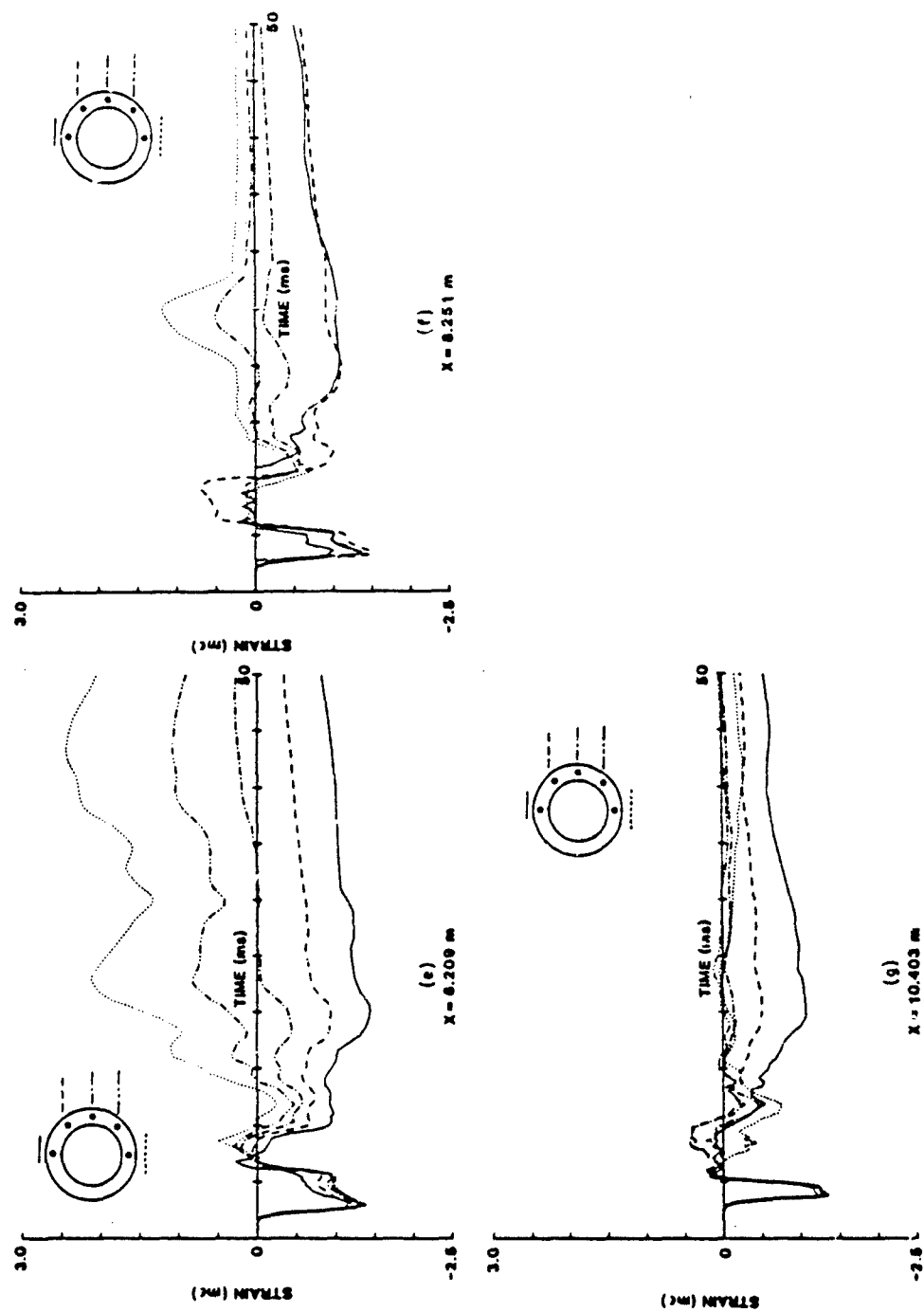


Figure 10. SAMSON structural axial strains (continued).

strain and for timing and magnitude of the bending moment. At  $X = 8.25$  meters Figure 9 (f) and 10 (f) both sets of data indicate a detour of the axial stress path from around the SALT port lid and concentrated between the bottom of the lid and springline. Tensile strain from the relief wave off of the backwall-soil interface also concentrates at this point. Also, the bending moment has substantially reduced in both sets of data (although more so in the test data). At  $X = 10.3$  meters (Figure 9 (g) and 10 (g)) the initial peak strain impulse is low and the bending moment has essentially disappeared in both sets of data. The SAMSON calculation underestimates the peak tensile strains due to the reflected relief wave, possibly, because the assumed R/C material (Figure 4) overestimates tensile capability.

#### Soil Response

DCT-2 test data relevant to the SAMSON calculation are in two categories; (1) longitudinal motion and (2) vertical motion.

##### Longitudinal Motion.

Soil deformation under a simulated nuclear environment can be very large. But under relatively short distances, attenuation of peak soil motion and stresses can also be very large. Therefore, unless a node point in a finite element grid is at the same relative location as a gage measurement in the testbed, the two resultant plots may be very different, and rightly so. The DCT-2 measured data is shown in Figure 11 compared to SAMSON data from nodes located on either side. The DCT-2 gage measurements were 0.7 meter (27.6 in) away from the structure, whereas the SAMSON soil nodes are immediately adjacent to and directly influenced by the structure. Due to the structure influence, the SAMSON data will have high early time velocity (when the structure initially punches through, dragging the soil back) and low late time peak velocity (when the structure retards the progression of the ground shock). Even the DCT-2 test data shows a hint of early time structural influence at  $X = 4.159$  meters and 6.209 meters (Figure 11 (b) and (c)).

##### Vertical Motion.

Figure 12 (a), (b), and (c) shows plots of free field soil vertical velocities at three different depths,  $Z = 0.250$  meter, 1.031 meters, and

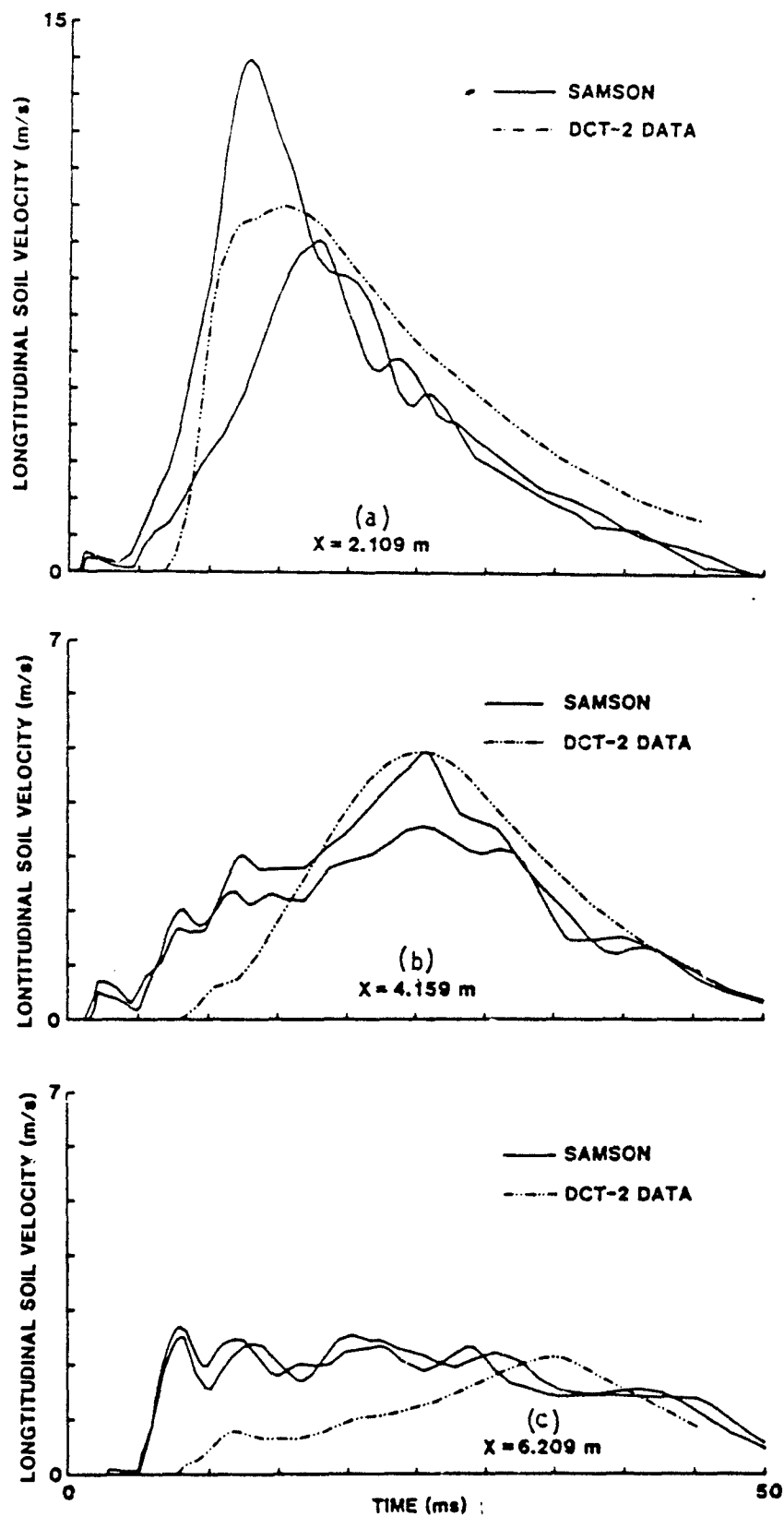


Figure 11. Longitudinal soil motions.

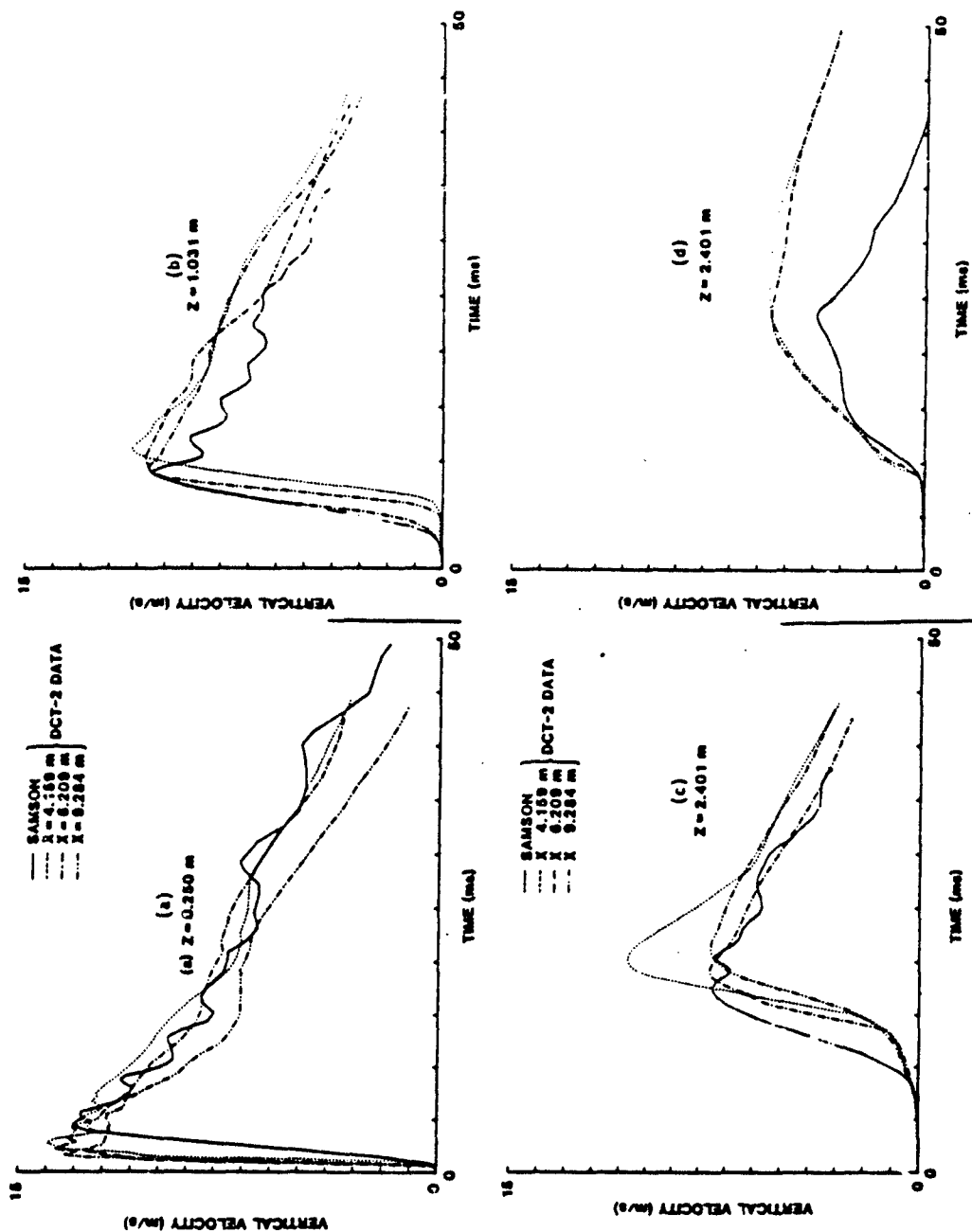


Figure 12. Comparison of vertical soil motions.

2.401 meters, respectively, for both the SAMSON calculation and DCT-2 test data. Figure 12 (d) shows plots of near field soil vertical velocities directly beneath the structure at a depth of  $Z = 2.401$  meters. The SAMSON data agrees very well with the free field test data. One DCT-2 free field test data measurement did not agree well with the others (the dotted line in Figure 12 (c)). There are a couple of possibilities for this odd measurement; (1) the gage measurement was incorrect or (2) the location of  $X = 4.159$  meters and  $Z = 2.401$  meters may be feeling the combined effects of the horizontal and vertical HEST cavities. Timing of the vertical and horizontal ground shock does not support the second possibility.

The peak vertical velocity of the near field test data at  $Z = 2.401$  meters (Figure 12 (d)) is 5.5 m/s, which is lower than the peak vertical velocity in the free field at the same depth (7.5 m/s, Figure 12 (c)). This is due to the shadowing effect of the structure on the vertical ground shock. The SAMSON calculation overestimates this shadowing effect and results in an even lower peak vertical velocity (4.0 m/s, Figure 12 (d)). The soil underneath the structure in the testbed is influenced by vertical soil flow around the structure. The SAMSON finite element grid has no way of accounting for this phenomenon.

#### SMI Normal Stress

Figure 13 shows plots of SMI normal stresses at the crown and invert at four locations down the length of the structure,  $X = 0.152$  meter, 0.652 meter, 6.209 meters, and 11.820 meters, respectively. At each location there is a plot of the crown normal stress (dash dot line), the invert normal stress (dotted line), and the sum of the two curves (solid line). Positive stress is a downward load on the structure. At  $X = 0.152$  meter (Figure 13 (a)) there is an overwhelming pressure load from underneath the structure trying to force the front portion of the structure up out of the soil. This high pressure region is caused by the airblast pressure loading on the front wall and is a result of the soil confinement. The soil over the crown is loaded in the same manner, but there is a nearby free air surface and the pressure in the soil is only able to develop to the transverse load airblast pressure. At  $X = 0.652$  meter (Figure 13 (b)) the high pressure region

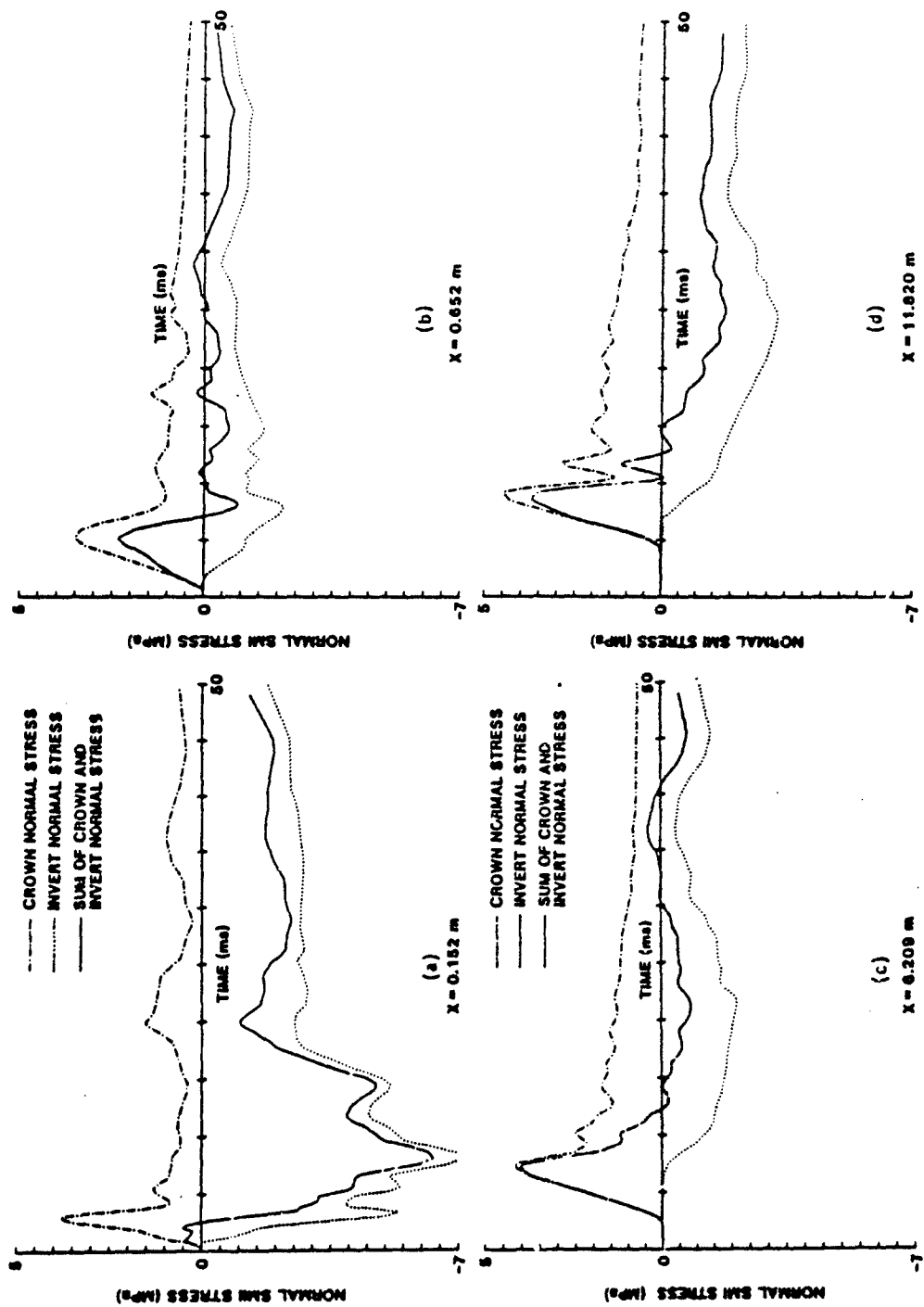


Figure 13. SMI normal stresses.

has disappeared. Here the pressure load is primarily downward. This is a moment couple which initiates moment wave traveling down the structure from front to rear. Figure 13 (c) shows a typical loading distribution for the center of the structure with the pressure load predominantly downward. But at the back (Figure 13 (d)) the pressure load shifts at late time (greater than 15.0 ms) to a predominant upward load again. This is the reaction pressure at the structure invert due to the vertical bending moment.

Figure 14 shows a comparison of crown SMI normal stresses for the SAMSON calculation (solid line) and test data (broken lines). At early time (prior to 5.0 ms) the SAMSON calculation does not match the spiked stresses in the test data. This is most likely due to the fact that the finite element grid is coarse and unable to transmit such high frequency response. The early time pressure spikes may be matched better with a fine grid. This coarse grid analysis assumes that such early time spiking is insignificant to overall structural response. After 5.0 ms the agreement between the two sets of data is excellent.

Figure 15 shows a comparison of invert SMI normal stresses for both sets of data. Here the agreement is also excellent. Both plots show a slow rise time to a peak stress of 2.4 MPa and then a slow decay (although the decay is more pronounced in the SAMSON data). The excellent match in the two sets of data shows that the ovaling model was very successful in filtering the load from the crown to the invert.

#### CONCLUSION

A quasi three-dimensional finite element modeling procedure of a horizontal buried shelter has been developed. This procedure is simple to use and inexpensive to run. It models structural response to include the initial longitudinal compressive wave, longitudinal vertical bending, and ovaling. It is extensive and reliable in information gained. The results of this analysis model closely the dynamic response of the structural field test data. This procedure can also be applied to vertical shelter response, particularly if one is concerned about bending of the longitudinal axis of the tube.

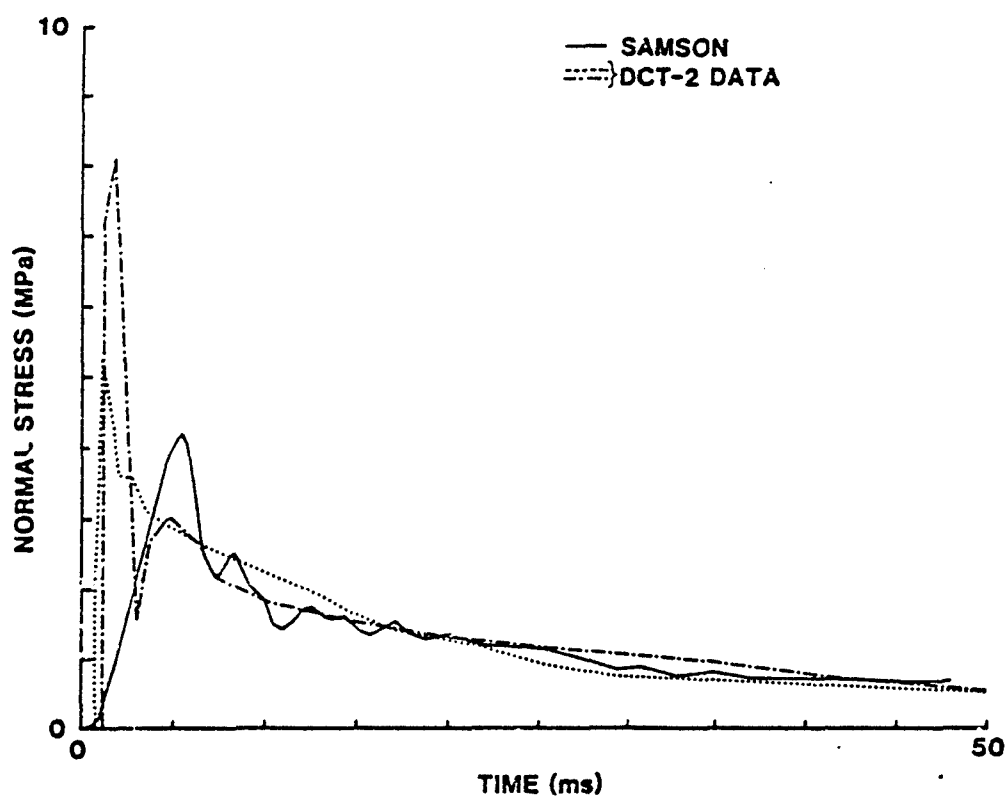


Figure 14. Crown normal SMI.

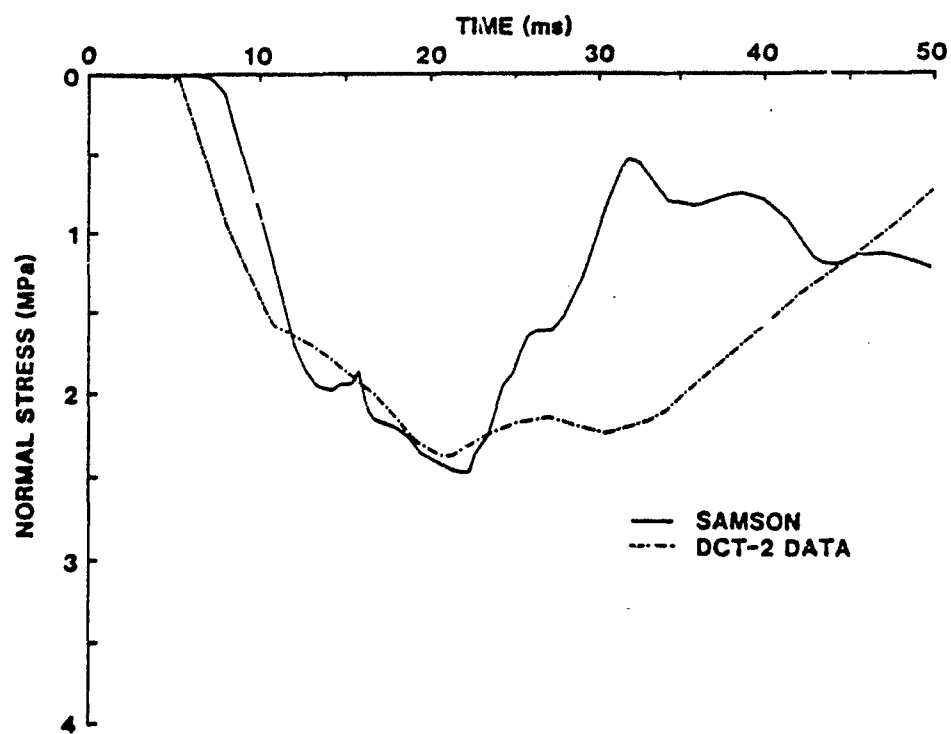


Figure 15. Invert normal SMI.

#### REFERENCES

1. Bartel, H. D., and Cole, D. M., "User Manual for SAMSON and Family," AFWL DE-TN-74-009, Air Force Weapons Laboratory, Kirtland AFB, New Mexico, 1974.
2. Timoshenko, S., and Woinowsky-Krieger, S., "Theory of Plates and Shells," Second Edition, McGraw-Hill Book Co., New York, 1959.

## SUMMARY

FINITE ELEMENT DYNAMIC ANALYSIS OF THE DCT-2 MODELS, by Barry L. Bingham. This report discusses a quasi three dimensional finite element analysis of a horizontal buried missile shelter. The analysis examines axial response to include longitudinal bending.

82-13  
AFCMD/PA  
Public Affairs  
KAFB, NM 87117